ACS NANO

ARTICLE

Role of Acid−Base Equilibria in the Size, Shape, and Phase Control of Cesium Lead Bromide Nanocrystals

Guilherme Almeida,[†,⊥] Luca Goldoni,[‡,§] Quinten Akkerman,[†,⊥] Zhiya Dang,[†] Ali Hossain Khan,[†] Sergio Marras,[∥] Iwan Moreels,[†,#] and Liberato Manna*,[†]

[†]Department of Nanochemistry, [‡]D3-PharmaChemistry Line, [§]Analytical Chemistry Facility, and [∥]Materials Characterization Facility, Istituto Italiano di Tecnologia, Via Morego 30, 16163 Genova, Italy

[⊥]Dipartimento di Chimica e Chimica Industriale, Università degli Studi di Genova, Via Dodecaneso, 31, 16146 Genova, Italy

[#]Department of Chemistry, Ghent University, Krijgslaan 281-S3, 9000 Gent, Belgium

Ⓢ Supporting Information

ABSTRACT: A binary ligand system composed of aliphatic carboxylic acids and primary amines of various chain lengths is commonly employed in diverse synthesis methods for $CsPbBr_3$ nanocrystals (NCs). In this work, we have carried out a systematic study examining how the concentration of ligands (oleylamine and oleic acid) and the resulting acidity (or basicity) affects the hot-injection synthesis of $CsPbBr_3$ NCs. We devise a general synthesis scheme for cesium lead bromide NCs which allows control over size, size distribution, shape, and phase ($CsPbBr_3$ or Cs_4PbBr_6) by combining key insights on the acid−base interactions that rule this ligand system. Furthermore, our findings shed light upon the solubility of $PbBr_2$ in this binary ligand system, and plausible mechanisms are suggested in order to understand the ligand-mediated phase control and structural stability of $CsPbBr_3$ NCs.

KEYWORDS: halide perovskites, $CsPbBr_3$, nanocrystals, acid−base, colloidal synthesis
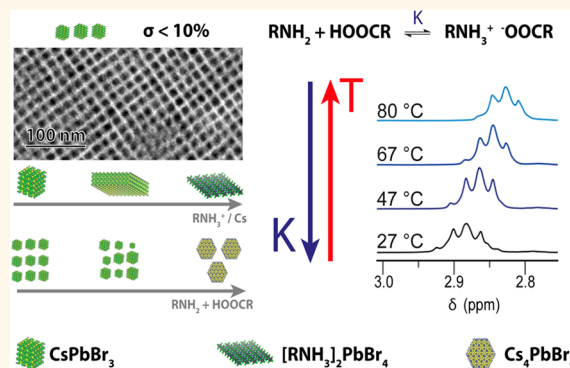
Lead halide perovskites (LHPs), with the formula $APbX_3$ (A = CH_3NH_3, Cs etc; X = Cl, Br, I), have been extensively researched over the past decade as active absorber materials for solar cells, with efficiencies now exceeding 22.1%.[1−3] Following the striking performances of thin-film LHPs, $CsPbX_3$ nanocrystals (NCs) were synthesized by Protesescu et al.[4] These $CsPbX_3$ NCs possess bright and easily tunable luminescence over the entire visible range, which makes them excellent candidates for photonic sources.[4−6] With respect to the traditional semiconductors that are typically used in these applications, LHPs offer potentially lower manufacturing costs by relying on solution-based processes.[7] However, still little is known about the underlying mechanisms that rule their formation, even though they are the key to improving quality standards and to the development of commercial formulations.[8−12]

Generally, LHP thin films, powders, and NCs are fabricated by precipitation reactions in aprotic solvents. In particular, the synthesis of NCs is conducted in a nonpolar solvent and often in the presence of a binary ligand system composed of aliphatic carboxylic acids and primary amines of various chain lengths.[4,13] In the common hot-injection synthesis of cube-shaped $CsPbBr_3$

NCs,[4] Cs-oleate is injected into a hot solution (190 °C) of $PbBr_2$, oleic acid (OA), oleylamine (OlAm), and 1-octadecene (ODE). Although this approach leads to strongly luminescent NCs, reports have also indicated a fast defocusing of the size distribution within a few seconds from the injection,[14] making it difficult to obtain samples with standard deviations below 15%, which are highly desirable for both device fabrication and fundamental studies. Moreover, size control was limited (8−12 nm) by the narrow workable temperature range, which was bound by the precipitation of $PbBr_2$ at ca. 195 °C and by the coformation of nanoplatelets (NPLs) below 150 °C.[4,8,15] Furthermore, accurate shape and thickness control of NPLs is yet to be achieved using the hot-injection method.[8,15] In this regard, a clearer understanding of the factors that regulate the formation of NPLs is needed in order to improve their quality. So far, their formation has not only been correlated to low temperatures[15] but also to the presence of short alkylamines[8]

and high concentrations of alkylammonium ions,[16,17] but there is no clear consensus on what the key driving factor is.

In this work, we demonstrate how the acid−base chemistry of the OlAm/OA binary ligand system is central to the size, shape, and phase control of cesium lead bromide NCs synthesized *via* the hot-injection method. We have found that increasing the concentration of ligands promotes Ostwald ripening but also allows the precipitation temperature of $PbBr_2$ to rise above 195 °C and to enable the synthesis of NCs in a temperature range (above 195 °C) that has hardly been explored to date. Furthermore, we confirmed that mixtures of oleic acid and oleylamine in a nonpolar medium lead to the protonation of oleylamine by oleic acid. Oleylammonium-rich synthetic conditions promoted anisotropic growth through a competition between oleylammonium and Cs^+ ions. The concentration of oleylammonium (RNH_3^+) could be increased not only by raising the concentration of oleic acid but also by lowering the temperature. By combining these key insights, we were able to prepare nanocubes from 4.0 nm (strongly quantum confined) to 16.4 nm (a range which is significantly wider than the 8−12 nm obtained by the standard approach[4]), with size distributions in the range of 8 to 15%. Larger sizes were also accessible, at the expense of a broader size distribution. Similarly, we could synthesize NPLs with controlled thicknesses, down to a single monolayer sheet with a $(RNH_3)_2PbBr_4$ composition. The phase of the NCs could be switched from $CsPbBr_3$ to the so-called zero-dimensional Cs_4PbBr_6, when working above a threshold concentration of ligands. This is explained in terms of the high solubility of $PbBr_2$ at high concentration of ligands, which shifts the $4CsPbBr_3 \leftrightarrow Cs_4PbBr_6 + 3PbBr_2$ equilibrium to the right. Finally, many of these findings could be successfully extended to the Cl and I systems.

SIZE, SHAPE, AND PHASE CONTROL OF CESIUM LEAD BROMIDE NCS

In this section, we will address the synthesis of NCs, specifically the acid−base conditions which enable control over size, shape, and phase. Mechanistic considerations will be discussed in the following sections. The $CsPbBr_3$ NCs reported in this work were all synthesized based on the method reported by Protesescu *et al.*,[4] and the size and shape control was obtained by only altering the reaction temperature and the concentrations of OA, OlAm, and Cs^+. In short, 72 mg of $PbBr_2$ (0.20 mmol, 33 mM) were dissolved in a 6.0 mL mixture of various concentrations of ligands (OlAm and OA) and solvent (ODE). After the $PbBr_2$ was dissolved at 100 °C under vacuum, the mixture was heated under nitrogen to the target reaction temperature, at which point 0.5 mL of a warm Cs-oleate solution was injected. This resulted in an instantaneous nucleation burst. Thereafter, samples were immediately cooled to room temperature with an ice bath and separated by centrifugation (see the Methods for additional details).

It is important to note that $PbBr_2$ is highly soluble in the binary ligand mixture (OlAm + OA) but not in OA or OlAm alone (as will be further discussed later). Under the conditions that are proposed by Protesescu *et al.* ([OA] = [OlAm] = 0.25 M), $PbBr_2$ precipitates when it is heated to a threshold temperature of 195 °C (XRD pattern shown in Figure S1 of the Supporting Information, SI).[4] By increasing the amount of ligands, we found that this precipitation temperature can be increased up to 290 °C, as shown in Figure 1, which allows for the synthesis of $CsPbBr_3$ NCs even at high temperatures.
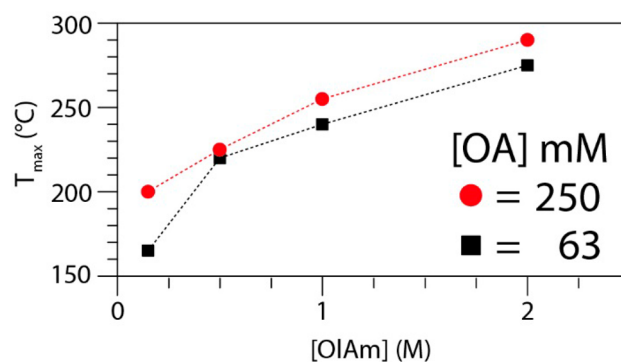

Figure 1. Maximum reaction temperature T_{max} as a function of ligand concentration; at T_{max}, $PbBr_2$ precipitates from the reaction medium (33 mM $PbBr_2$ solution in ODE with [OA] set at a constant of 63 and 250 mM).

Furthermore, we found that keeping the concentration of ligands close to the minimum amount needed to solubilize the $PbBr_2$ enabled the synthesis of nanocubes with narrow size distributions (Figure 2a).

Examples of NCs that we could synthesize with our general scheme are reported in Figure 2: 4.0 to 7.6 nm cubes ($\sigma = 8−13\%$) were prepared at 120−150 °C in the presence of 0.25 M OlAm and 25 mM OA. Larger cubes were obtained by increasing the reaction temperature, which also required increasing the concentration of ligands. For instance, 16.4 nm cubes ($\sigma = 15\%$) were obtained at 220 °C. Syntheses carried out at 240 °C ([OlAm] = [OA] = 1.5 M) delivered even larger nanocubes (beyond 100 nm), but they had a very broad size distribution (see Table 1 and Figure S2 of the SI). All nanocubes synthesized with our approach had crystal structures that matched the orthorhombic $CsPbBr_3$ phase (Figure 2d), narrow photoluminescence (PL) peaks (full-widths at half-maximum of 70−100 meV for weakly confined samples, 140−170 meV for strongly confined samples, which is in agreement with other reports),[4,18] and high PL quantum yields (Table 1).

Our strategy of synthesizing $CsPbBr_3$ nanocubes by using the minimum amount of ligands needed to solubilize $PbBr_2$ also suppressed Ostwald ripening, which normally leads to the fast defocusing of NC size within seconds after the injection of Cs^+. The suppression of Ostwald ripening was clear, since nearly monodisperse NCs could even be obtained when the reaction was allowed to cool without an ice bath, *i.e.*, solely by removing the heating mantle, a procedure that normally requires at least 10 min for the flask to cool down (see Figure 2f). Furthermore, under such reduced concentrations of ligands, the formation of nanoplatelets was never observed, regardless of the reaction temperature. Rather, the amount of NPLs increased when the concentration of oleic acid in the reaction mixture was increased (see Figure S3). Following this observation, pure, square-shaped (ca. 10 × 10 nm, 2.4 nm thick) $CsPbBr_3$ NPLs were prepared at 140 °C by increasing the concentration of oleic acid in the reaction mixture (from 25 mM to 0.5 M) as well as in the injection solution (see Figure S4). The thickness of the NPLs could be reduced by decreasing the amount of Cs^+ injected (while keeping the amount of OA constant, see Table S2), as is evidenced by the absorbance and PL spectra of the samples (Figure 2b,c, bottom 3). Similar to the findings in previous reports,[17,19] the NPLs exhibited narrow PL peaks (Figure 2c) and their structural anisotropy was evidenced by strong ($hk0$) reflections in their XRD patterns (Figure 2d; see
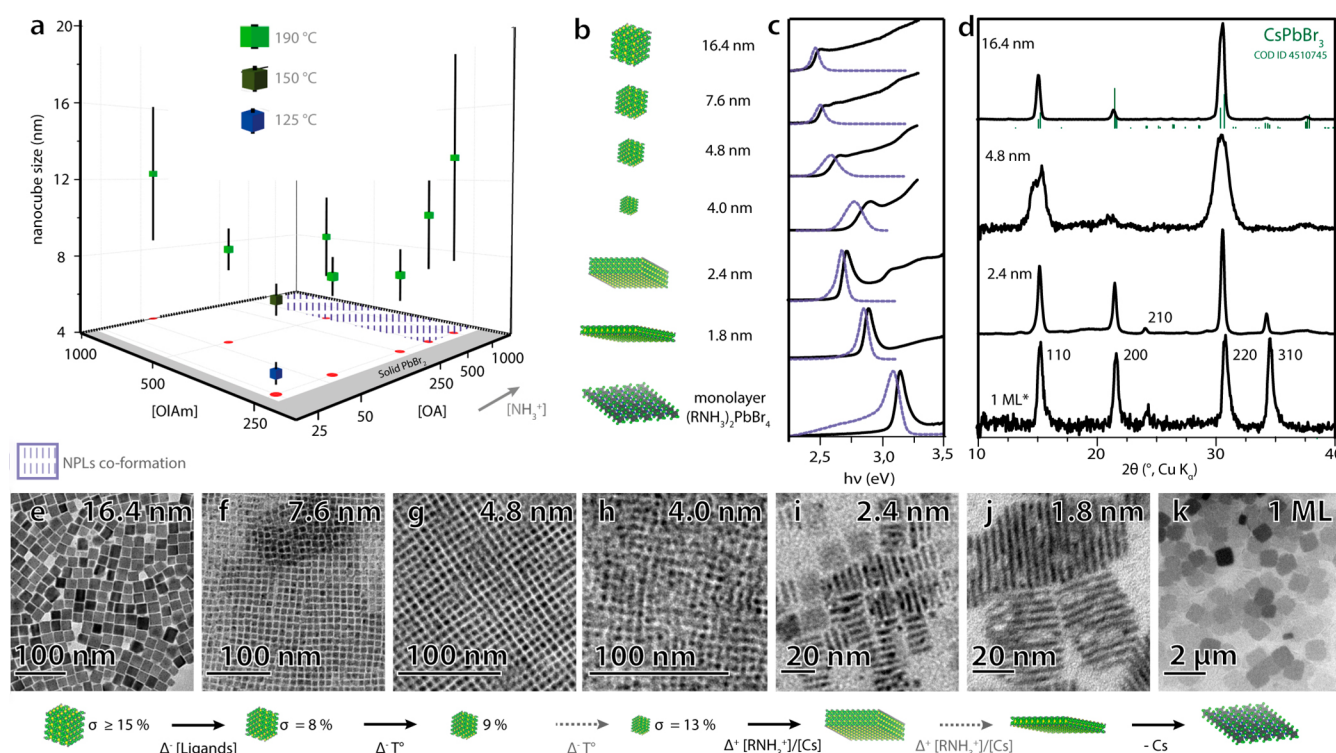
Figure 2. (a) Sizes of CsPbBr$_3$ nanocubes synthesized using various concentrations of oleylamine (OlAm) and oleic acid (OA) and different reaction temperatures (size distributions are represented as vertical bars across each symbol). (b) Image illustrating the range of monodisperse CsPbBr$_3$ nanocubes, nanoplatelets, and nanosheets synthesized in this work using only OlAm and OA as ligands. (c) Absorbance (black solid line) and photoluminescence (blue dashed line) spectra. (d) XRD patterns and (e–k) TEM images of the depicted samples.

Table 1. Synthesis Conditions Used To Prepare the CsPbBr$_3$ Nanocubes and Their Photoluminescence (PL) Properties[a]

NC size		reaction conditions			photoluminescence (PL)			
M (nm)	σ (%)	T (°C)	[OlAm] (mM)	[OA] (mM)	$h\nu$ (eV)	fwhm (meV)	ϕ (%)	τ (ns)
>100	n/a	240	3500	3500				
16.4	15	220	500	500	2.39	69	30	45.1
8.7	26	190	500	500	2.41	83		
13.2	41	190	250	1000	2.41	103		
10.3	26	190	250	500	2.41	84		
7.6	16	190	250	250	2.41	80		
8.1	10	190	250	63	2.42	75		
8.6	12	190	500	63	2.41	74		
12.3	31	190	1000	63	2.41	83		
7.6	8	150	250	25	2.43	79	49	7.6
4.8	9	125	250	25	2.53	136	27	5.2
4.0	13	120	250	25	2.60	170	24	3.5

[a]Key: μ, mean size; σ, standard deviation; T, synthesis temperature; $h\nu$, photon energy at PL maximum; FWHM, PL full width at half maximum; φ, PL quantum yield; τ, PL lifetime; –, data not collected. All syntheses were immediately quenched upon injection of 0.5 mL of Cs-oleate (0.15 M, in 1-octadecene) except the >100 nm sample where 2 mL of Cs-precursor was used and the growth time was increased to 60 s.

Figure S5 for a representative high-resolution transmission electron microscopy image).

Interestingly, when Cs$^+$ ions were not included in the injection solution, a white precipitate formed upon cooling. This precipitate consisted of micron-sized nanosheets whose crystal phase could be assigned to that of a hybrid organic–inorganic two-dimensional perovskite slab with the formula (RNH$_3$)$_2$PbBr$_4$, in which RNH$_3$ denotes the oleylammonium ion (the corresponding XRD pattern is the first one from the bottom in Figure 2d). Its PL spectrum (Figure 2c, bottom row) is characterized by a peak at 3.09 eV, with a long tail to lower

energies, which is in agreement with previous reports for two-dimensional perovskites.[20,21]

We have also observed that by increasing the concentrations of both oleic acid and oleylamine in the reaction mixture, we could synthesize NCs in the lead-poor hexagonal Cs$_4$PbBr$_6$ phase (Figure 3c–e), which is a nonluminescent insulator characterized by a strong and narrow absorption band resembling that of individual [PbBr$_6$]$^{4-}$ clusters (Figure 3a,b).[22,23] A similar result was observed by treating CsPbBr$_3$ NCs with an excess of these same ligands (OA and OlAm), as their phase changed to Cs$_4$PbBr$_6$. In this case, 8 nm cube-
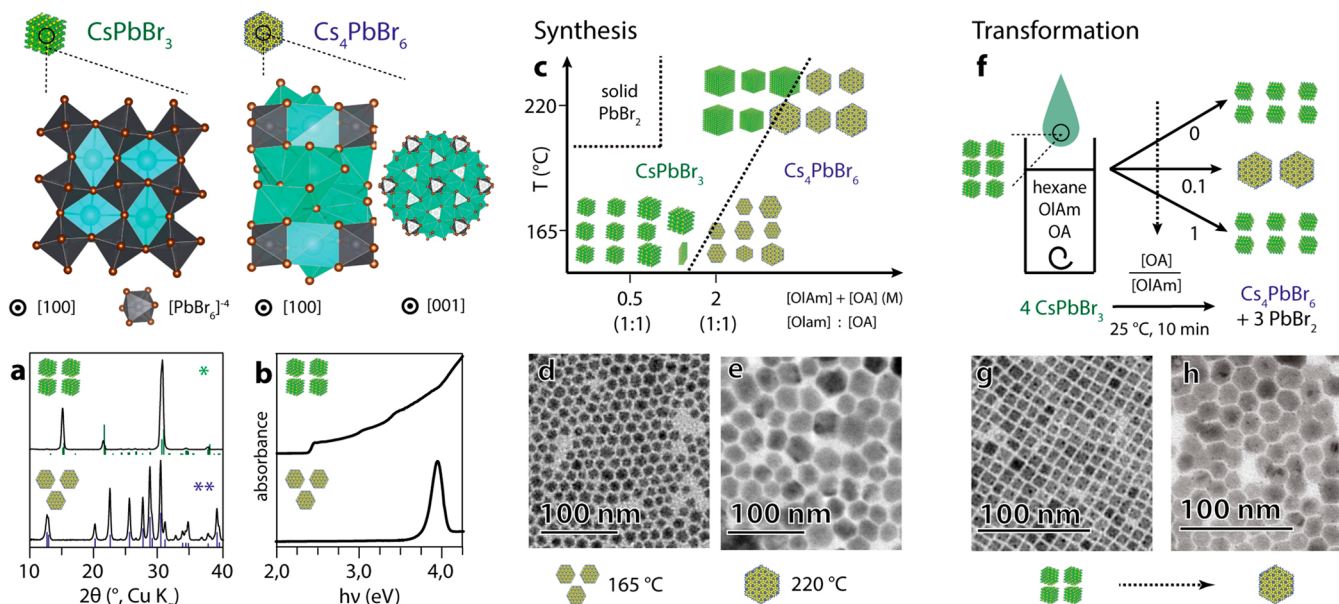
Figure 3. Ligand-mediated synthetic and postsynthetic phase control of cesium lead bromide NCs (OlAm = oleylamine, OA = oleic acid). (a) Typical XRD patterns and (b) absorbance spectra of CsPbBr$_3$ and Cs$_4$PbBr$_6$ NCs (*COD 4510745; **ICSD 98-009-7851). (c) Scheme depicting how the interplay between the reaction temperature and ligand concentration affects the crystal structure and, hence, the composition of the obtained NCs. TEM image of Cs$_4$PbBr$_6$ NCs synthesized at (d) 165 °C and (e) 220 °C. (f) Scheme depicting the ligand-driven transformation of CsPbBr$_3$ NCs into Cs$_4$PbBr$_6$ NCs: in short, 100 μL of a dispersion containing CsPbBr$_3$ nanocubes was added to a solution (1.0 mL), kept under stirring, that contained a fixed concentration of OlAm (0.4 M) and various concentrations of OA and solvent (hexane). This transformation was followed by spectroscopy analysis, and the transformation rate was found to be modulated by the [OA]/[OlAm] ratio, as shown in the figure above. For the sake of simplicity, only the state of the systems at t = 10 min is shown. TEM images of NCs (g) before and (h) after the transformation.
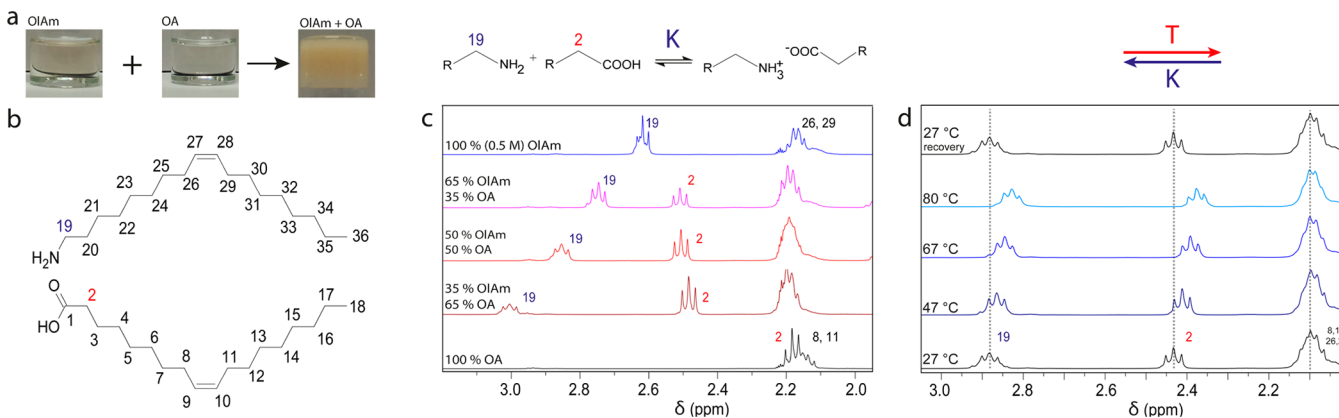

Figure 4. (a) Photographs illustrating the formation of the oleylammonium oleate salt. (b) Structure of oleylamine (OlAm) and oleic acid (OA). (c) Selected regions of the ^{1}H NMR spectra of OlAm and OA solutions in toluene-d_8. (d) ^{1}H NMR spectra of a mixture of OlAm and OA in toluene-d_8, recorded at different temperatures in the range of 27 to 80 °C (upfield shifts are observed for the α-CH$_2$ ^{1}H NMR resonances 19 and 2, while all the other signals, e.g., 8, 11, 26, and 29, remain unchanged). All resonances identified are in agreement with previous works.[32,33]

shaped CsPbBr$_3$ NCs could be transformed to ca. 20 nm hexagonal Cs$_4$PbBr$_6$ NCs. This increase in NC size is in agreement with the two-step dissolution−recrystallization mechanism that is reported in previous works.[24,25] Interestingly, the rate of this transformation was found to be dictated by the ratio between OA and OlAm and will be discussed in the next section.

DISCUSSION

Acid−base Equilibrium. This section discusses the acid−base chemistry of OlAm and OA mixtures in nonpolar solvents and how the size, shape, and phase control of cesium lead bromide NCs are regulated. It is known that, in aprotic solvents, partially substituted nitrogen bases and carboxylic acids can form hydrogen bonded ionic salts.[26] The first hint of the formation of ammonium carboxylate salts can be observed by simply mixing OlAm (base, B) and OA (AH) in a 1:1 molar ratio at room temperature. This generates heat and leads to the formation of a gel (Figure 4a), indicating that the ions mainly associate in their salt form under these conditions.

$$B + H - A \leftrightarrow BH^+ \cdots A^- \qquad (1)$$

To confirm the formation of this ammonium carboxylate, nuclear magnetic resonance (NMR) analysis was performed on

OlAm and OA mixtures in toluene-d_8 (Figure 4c). In the presence of an excess of OA, the α-CH$_2$ resonances of OlAm (19) exhibit a downfield shift in the ^{1}H NMR spectrum, which occurs as a consequence of the nitrogen protonation, while the α-CH$_2$ resonances of OA (2) show a downfield shift with the deprotonation of the carboxylic acid (Figure 4b). Opposite shifts are observed in the ^{13}C NMR spectrum; *i.e.*, upfield shifts occur for the α-CH$_2$ carbon of both the OlAm and the OA as a result of the protonation of the adjacent functional group (Figure S7.2). In the SI, section S6, we report the complete assignment of the components in a model mixture of 0.5 M OlAm and 1 M OA in toluene-d_8. The α-CH$_2$ resonances of OlAm (19) and those of OA (2) were unambiguously identified by the ^{1}H−^{13}C-HMBC NMR spectrum (Figure S6.1d).

As previously mentioned, the formation of the ammonium carboxylate is exothermic, which implies, on the basis of Le Chatelier's principle, that the equilibrium will shift toward the reactants when the temperature is increased. This was also confirmed by ^{1}H NMR spectroscopy. Notably, the α-CH$_2$ ^{1}H NMR resonances of the protonated OlAm (19) and those of OA (2) shifted upfield when the temperature was increased, which confirms the deprotonation of the oleylammonium ions and the protonation of the carboxylic acid (Figure 4d). These facts have important implications in the colloidal synthesis and phase stability of CsPbBr$_3$ NCs, as will be outlined in the next section.

Role of Ligands in Size and Shape Control. First, we re-emphasize the fact that both ligands are necessary to solubilize solid PbBr$_2$, which highlights the active role of both the ammonium and carboxylate species in this process. In this system, PbBr$_2$ exhibits an inverse solubility behavior (see Figure 1) that is related to the decrease in the concentration of ammonium and carboxylate species when the temperature is increased, as has been previously demonstrated. In addition, we found that this binary ligand mixture can also dissolve CsPbBr$_3$ NCs (Figure 3f−h). This phenomenon is in agreement with the strong Ostwald ripening effects that were observed during the NC growth.[14] Accordingly, we found that Ostwald ripening could be suppressed by reducing the concentration of ligands, as is evidenced by the narrower size distributions of the NCs that were obtained following our strategy (Figure 2).

Second, it is now well established that aliphatic ammonium (RNH$_3^+$) ions can compete with Cs$^+$ ions for lattice sites and promote the formation of hybrid layered structures with the general formula [RNH$_3$]$_2$[CsPbBr$_3$]$_{n-1}$PbBr$_4$ (in which n denotes the number of PbBr$_6$ octahedra along the thickness).[27,28] Indeed, our results in terms of shape control showed that NPLs could be obtained by increasing the [RNH$_3^+$]/[Cs$^+$] ratio. Following this concept, and accounting the temperature dependence of [RNH$_3^+$], pure NPL samples could be synthesized even at high temperatures (190 °C) by simply adjusting the [Cs$^+$] accordingly (see Table S2 and Figure S7). Moreover, such two-dimensional hybrid systems could also be synthesized in the presence of other Brønsted acids. Notably, when the acid strength increased (benzylsulfonic ≫ hexanoic > oleic acid), lower amounts of acid were needed to begin forming such structures (Figure S8).

Mechanistic Insights. The solubility of PbBr$_2$ in this system can be interpreted on the basis of the dissociation of the oleylammonium oleate salt followed by the solvation of PbBr$_2$. In addition to thermal effects, the dissociation of acid base salts in aprotic solvents can also occur *via* homoconjugation

$$BH^+{\cdots}A^- + B \leftrightarrow (BH^+{\cdots}B)A^- \tag{2}$$
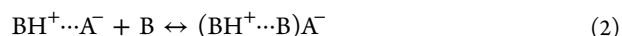
a mechanism that typically shows high equilibrium constants for amine-based systems.[26,29−31]

The interpretation of the oleylammonium oleate salt as an inactive species is supported by our results in terms of phase transformation (Figure 3f−h). In short, the transformation of CsPbBr$_3$ into Cs$_4$PbBr$_6$ is driven by the ability of the ligand mixture to solubilize PbBr$_2$, which is the byproduct of this transformation. Our results demonstrate that the kinetics of this reaction is modulated by the relative amounts of acid and base (Figure 3f). The transformation does not proceed in the absence of acid but is found to be completed in a few minutes when the amount of acid is ca. 10% mol of that of the amine. However, increasing the concentration of acid any further slows down the transformation until it does not proceed again. Therefore, at room temperature, a 1:1 molar mixture of oleylamine and oleic acid, which mainly exist in salt form, gelates in the absence of a solvent. However, when an excess of base is present, it can dissociate into ionic species which, in turn, can dissolve PbBr$_2$ and drive the transformation.

Furthermore, we found that PbBr$_2$ (1 equiv) can be dissolved at mild temperatures (ca. 80−100 °C) in the presence of a minimum amount of 0.5 equiv of stearic acid and an excess of amine ligands (4−5 equiv) (here, octadecylamine and stearic acid were used due to their high purity), which is likely a result of the partial dissociation of PbBr$_2$:

$$2PbBr_2 + BH^+{\cdots}A^- + xB \rightarrow PbBr_3^-{\cdot}BH^+ + PbBr^+{\cdot}A^- + xB \tag{3}$$
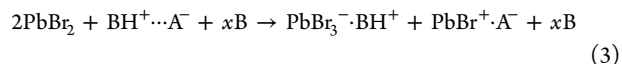
Note that the solubility of PbBr$_2$ in polar aprotic solvents increases in the presence of methylammonium bromide, and recent computational studies have related this phenomenon to the formation of PbBr$_3$−methyammonium species with an increased stability.[9]

Our results, in terms of phase control (Figure 3c-e), demonstrate that the NCs tend to crystallize in the lead-poor Cs$_4$PbBr$_6$ phase when both ligands are present in large excess. Under such conditions, a full dissociation of the lead salt into lead oleate and oleylammonium bromide is likely to occur:

$$PbBr_2 + 2(BH^+{\cdots}B)A^- \rightarrow Pb{\cdot}A_2 + 2(BH^+{\cdots}Br^-) + 2B \tag{4}$$
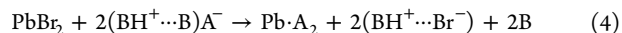
This system allows a greater degree of freedom than the one described by eq 2 with respect to possible outcomes upon the injection of Cs$^+$ ions. For instance, the reaction of an alkylammonium bromide with Cs$^+$ in the same ligand mixture results in the formation of CsBr NCs (Figure S9). The two extreme situations illustrated in eqs 3 and 4 can thus explain our results in terms of ligand-mediated phase control. Again, given the temperature profile of the acid base-equilibrium, a system described by eq 4 should shift to the one described by eq 3 when the temperature is increased. Indeed, we could find a ligand concentration that yields Cs$_4$PbBr$_6$ NCs at low temperatures (165 °C), and CsPbBr$_3$ NCs at high temperatures (220 °C, Figure 2c).

Extension to Other Halide Systems. Most of the findings reported herein were also found to be valid for the Cl and I systems. For instance, PbCl$_2$ and PbI$_2$ also exhibit inverse solubility in this binary ligand system, and the reprecipitation temperatures follow a similar trend to that found for PbBr$_2$ (see Figure S11). Furthermore, CsPbX$_3$ NCs, Cs$_4$PbX$_6$ NCs, and (RNH$_3$)$_2$PbX$_4$ nanosheets (X = Cl, I) could also be synthesized following the same strategies presented here for the phase and

shape control of bromides (see Figures S12 and S13). Unfortunately, for the Cl and I cases, due to the poorer solubility of $PbCl_2$ and the lower reprecipitation temperature of PbI_2 in this binary ligand system, we could not reproduce the low ligand concentration conditions which had enabled us to synthesize $CsPbBr_3$ nanocubes with narrow size distributions.

CONCLUSION

In this work, we have shown how the acid−base interactions within a ligand system that consists of aliphatic primary amines and carboxylic acids affect the synthesis and transformation of cesium lead bromide nanocrystals in nonpolar solvents. This allowed us not only to achieve precise control over the size, shape, and phase of the nanocrystals but also to understand the solubility behavior of $PbBr_2$ in this system. In addition, many of the findings reported herein were also found to be valid for the Cl and I systems. Furthermore, one should be able to extend these observations to nonprotic polar solvents such as dimethylformamide, a commonly used solvent in the synthesis of lead halide perovskites, which is known to self-decompose into dimethylamine and formic acid[12] and is able to sustain the growth of perovskite single crystals *via* inverse solubility. Finally, the fact that this binary ligand system is able to dissolve $CsPbX_3$ nanocrystals and cannot provide good surface passivation[34] should prompt further studies into other ligand systems.

METHODS

Materials. $PbCl_2$ (≥99%) was purchased from Strem Chemicals. $PbBr_2$ (≥98%), PbI_2 (≥99.999%), oleylamine (70%, OlAm), octadecylamine (≥98%), oleic acid (90%, OA), stearic acid (95%), hexanoic acid (≥99%, HA), benzenesulfonic acid (≥94%, BSA), didodecyldimethylammonium bromide (≥98%, DDAB), 1-octadecene (90%), toluene (≥99.7%), toluene-d_8 (99 atom. % D), hexane (≥95%), 2-propanol (≥99.8%), and methyl acetate (anhydrous, 99.5%) were purchased from Sigma-Aldrich. All chemicals were used without any further purification unless otherwise stated.

Preparation of Cs-Oleate Precursors. *Solution 1. Cs-Oleate in 1-Octadecene (Cs_2CO_3/OA = 26% wt).* Cs_2CO_3 was weighed inside a 3-neck round-bottom flask along with oleic acid and 1-octadecene. The mixture was degassed under vacuum at 100 °C for 2 h in order to obtain a colorless Cs-oleate solution which was then transferred into the glovebox. Typically, 407 mg Cs_2CO_3, 1.55 g OA and 11.7 g ODE were combined to obtain a 0.15 M Cs-oleate solution.

Solution 2. Cs-Oleate in Oleic Acid. Cs_2CO_3 was weighed inside a three-neck round-bottom flask along with oleic acid (see Table S1 for concentrations). The mixture was degassed under vacuum at 100 °C for 2 h in order to obtain a colorless Cs-oleate solution which was then transferred into the glovebox. Diluted solutions were prepared inside the glovebox by dilution with degassed oleic acid.

Syntheses (General Considerations). All synthetic procedures were undertaken by employing standard Schlenk line techniques assisted by a nitrogen-filled glovebox where lead(II) bromide and the Cs precursors were stored. Syntheses were performed in 25 mL 3-neck round-bottom flasks equipped with a thermocouple and a magnetic stirrer at 800 rpm.

Synthesis of Cube-Shaped $CsPbBr_3$ Nanocrystals (NCs). All NCs were synthesized in 6.0 mL solutions containing 72 mg of $PbBr_2$ (0.2 mmol, 33 mM) and various amounts of oleylamine, oleic acid, and 1-octadecene (see Table 1). Mixtures were degassed for 15 min at 100 °C in order to obtain colorless solutions. Thereafter, the temperature was ramped to the desired value under a dry nitrogen flow and 0.5 mL of a 0.15 M Cs-oleate solution in 1-octadecene (solution 1, which had previously been heated for 10 min on a hot-plate set at 200 °C) was swiftly injected. Unless otherwise stated, the solutions were immediately cooled after injection with an ice bath and diluted with

5 mL of toluene. The dispersions were centrifuged at 2500 rpm (for 3 min) and the NCs were redispersed in 2.0 mL of hexane. 4.0 and 4.8 nm nanocubes could not be separated by centrifugation alone (even at 14 krpm). In both these cases, 1 mL of oleic acid was added to the dispersion (to assist the precipitation process) and the particles were then precipitated by adding methyl acetate until the solution became slightly turbid. The NCs were separated by the same centrifugation and redispersion steps. NCs smaller than 4.0 nm could also be synthesized (at temperatures under 120 °C), but they could not be isolated from solution by centrifugation alone, and the addition of antisolvents led to the formation of nanowires (see Figure S10).

Synthesis of Two-Dimensional $[RNH_3]_2[CsPbBr_3]_{n-1}PbBr_4$ Nanocrystals. The general procedure consisted in performing the nanocube synthesis under a high concentration of oleylammonium species ([OlAm] = 0.25 M and [OA] = 0.50 M) and varying the concentration of Cs^+ (the smaller the $[Cs^+]$, the thinner the crystals). Note that in this case the injection solution consisted of 0.5 mL of a solution of Cs-oleate in oleic acid (solution 2, $0 \leq [Cs^+] \leq 300$ mM) and that the growth times ranged from 1 to 5 min; a complete description of the reaction conditions is provided in Table S1 of the SI. Also note that the 1.7 nm thick nanoplatelets (NPLs) tend to transform into 2.3 nm thick NPLs upon dilution, which did not allow us to investigate their photoluminescence quantum yields.

$CsPbBr_3$ to Cs_4PbBr_6 Transformation Reactions. 100 μL of a nanocube dispersion ([Pb] = 13 mM, as measured by ICP) was injected into a stirring hexane solution containing oleylamine (0.4 M) and oleic acid (of various concentrations) with a total volume of 1.0 mL. Aliquots were collected over time in hexane in order to follow their transformation spectroscopically. The transformed NCs were separated by centrifugation and redispersed in hexane or toluene for further analysis.

Inductively Coupled Plasma−Optical Emission Spectroscopy (ICP−OES). The concentration of NC dispersions in Pb was determined by ICP-OES on a aiCAP 6000 spectrometer (Thermo Scientific). The NC solutions were digested in aqua regia overnight prior to the measurements.

X-ray Diffraction (XRD). Samples were prepared by drop-casting concentrated dispersions onto a zero diffraction silicon substrate. XRD measurements were conducted on a PANalytical Empyrean X-ray diffractometer equipped with a 1.8 kW Cu Kα ceramic X-ray tube and PIXcel3D 2 × 2 area detector, operating at 45 kV and 40 mA. The diffraction patterns were collected in air at room temperature using parallel-beam (PB) geometry and symmetric reflection mode. Due to preferential orientation, the diffraction pattern of the $(RNH_3)_2PbBr_4$ nanosheets was collected using an in-plane geometry on a Rigaku SmartLab 9 kW with the X-ray source operated at 40 kV and 150 mA.

Transmission Electron Microscopy (TEM). Bright field TEM images were acquired on a JEOL JEM-1011 microscope (W filament) operating at an accelerating voltage of 100 kV. For this purpose, samples were prepared by drop-casting dispersions on carbon-coated 200 mesh copper grids. High-resolution TEM (HRTEM) and high-angle annular dark field scanning (HAADF) images were acquired on a JEOL JEM-2200FS microscope, operating at 200 kV. The microscope is equipped with a CEOS objective corrector, allowing a resolution below 0.9 Å, and an in-column filter (Ω-type), which was used to increase the contrast in the images by filtering around the elastically transmitted electrons. To obtain a top-view and side-view of the NCs, the samples were drop-cast on ultrathin carbon on holey carbon coated 400 mesh copper grids.

Nuclear Magnetic Resonance. All spectra were acquired on a Bruker Avance III 400 MHz spectrometer, equipped with a Broad Band Inverse probe (BBI). Before each acquisition, automatic routines optimized the matching, tuning, resolution and 90 deg pulse calculation on ^{1}H nucleus.

^{1}H NMR: 16 transients were accumulated, without steady state scans, at 300 K, over a spectral width of 20.55 ppm (offset at 6.175 ppm), at a fixed receiver gain (64), using 30 s of inter pulse delays.

^{1}H NMR at different temperatures (from 300 to 353 K): 16 transients were accumulated, with 4 steady state scans, over a spectral

width of 20.55 ppm (offset at 6.175 ppm), at a fixed receiver gain (64), using 2.5 s of relaxation delay.

^{13}C NMR: 10240 transients were accumulated after a 30 degree pulse and 4 steady state scans, at 300 K, over a spectral width of 239 ppm (offset at 100 ppm), using 2.2 s of inter pulse delays. The receiver was automatically optimized.

All NMR chemicals shifts were referred to the not deuterated toluene residue peak at 7.09 ppm and 129.24 ppm at ^{1}H- and ^{13}C-NMR, respectively.

Steady-State UV–vis Extinction and Photoluminescence Spectroscopy. Optical extinction and photoluminescence spectra of hexane dispersions were recorded in quartz cuvettes with a 1 cm path-length, employing a Varian Cary 300 UV–vis spectrophotometer and a Varian Cary Eclipse fluorescence spectrophotometer, respectively.

Photoluminescence Quantum Yields and Time-Correlated Single-Photon Counting. The time-resolved photoluminescence spectra were measured using an Edinburgh Instruments FLS920 spectrofluorometer. The PL decay traces were recorded by exciting the samples at 405 nm using a 50 ps laser diode. The data were collected at the PL peak position with an emission bandwidth of 10 nm. The photoluminescence quantum efficiencies were measured using the same instrument with an integrating sphere, exciting the nanocrystal solution at 400 nm. The optical density of the nanocrystal solution was 0.1 at 400 nm.

ASSOCIATED CONTENT

Ⓢ Supporting Information

The Supporting Information is available free of charge on the ACS Publications website at DOI: 10.1021/acsnano.7b08357.

Synthetic details, control, and synthesis of CsBr NCs; additional structural characterization of NPLs (high-resolution transmission electron microscopy); additional NMR characterization of OlAm/OA solutions (^{13}C, ^{1}H–^{13}C-HSQC, and ^{1}H–^{13}C-HMBC spectra) (PDF)

AUTHOR INFORMATION

Corresponding Author
*E-mail: liberato.manna@iit.it.

ORCID Ⓘ
Iwan Moreels: 0000-0003-3998-7618
Liberato Manna: 0000-0003-4386-7985

Notes
The authors declare no competing financial interest.

REFERENCES

(1) Kojima, A.; Teshima, K.; Shirai, Y.; Miyasaka, T. Organometal Halide Perovskites as Visible- Light Sensitizers for Photovoltaic Cells. *J. Am. Chem. Soc.* **2009**, *131*, 6050–6051.

(2) Park, N.-G.; Grätzel, M.; Miyasaka, T.; Zhu, K.; Emery, K. Towards Stable and Commercially Available Perovskite Solar Cells. *Nat. Energy* **2016**, *1*, 16152.

(3) Yang, W. S.; Park, B.-W.; Jung, E. H.; Jeon, N. J.; Kim, Y. C.; Lee, D. U.; Shin, S. S.; Seo, J.; Kim, E. K.; Noh, J. H.; Seok, S., Il. Iodide Management in Formamidinium-Lead-Halide−based Perovskite Layers for Efficient Solar Cells. *Science* **2017**, *356*, 1376–1379.

(4) Protesescu, L.; Yakunin, S.; Bodnarchuk, M. I.; Krieg, F.; Caputo, R.; Hendon, C. H.; Yang, R. X.; Walsh, A.; Kovalenko, M. V. Nanocrystals of Cesium Lead Halide Perovskites (CsPbX$_3$, X = Cl, Br, and I): Novel Optoelectronic Materials Showing Bright Emission with Wide Color Gamut. *Nano Lett.* **2015**, *15*, 3692–3696.

(5) Nedelcu, G.; Protesescu, L.; Yakunin, S.; Bodnarchuk, M. I.; Grotevent, M. J.; Kovalenko, M. V. Fast Anion-Exchange in Highly Luminescent Nanocrystals of Cesium Lead Halide Perovskites (CsPbX$_3$, X = Cl, Br, I). *Nano Lett.* **2015**, *15*, 5635−5640.

(6) Sutherland, B. R.; Sargent, E. H. Perovskite Photonic Sources. *Nat. Photonics* **2016**, *10*, 295−302.

(7) Bush, K. A.; Palmstrom, A. F.; Yu, Z. J.; Boccard, M.; Cheacharoen, R.; Mailoa, J. P.; McMeekin, D. P.; Hoye, R. L. Z.; Bailie, C. D.; Leijtens, T.; Peters, I. M.; Minichetti, M. C.; Rolston, N.; Prasanna, R.; Sofia, S.; Harwood, D.; Ma, W.; Moghadam, F.; Snaith, H. J.; et al. 23.6%-Efficient Monolithic Perovskite/Silicon Tandem Solar Cells With Improved Stability. *Nat. Energy* **2017**, *2*, 17009.

(8) Pan, A.; He, B.; Fan, X.; Liu, Z.; Urban, J. J.; Alivisatos, A. P.; He, L.; Liu, Y. Insight into the Ligand-Mediated Synthesis of Colloidal CsPbBr$_3$ Perovskite Nanocrystals: The Role of Organic Acid, Base, and Cesium Precursors. *ACS Nano* **2016**, *10*, 7943−7954.

(9) Stevenson, J.; Sorenson, B.; Subramaniam, V. H.; Raiford, J.; Khlyabich, P. P.; Loo, Y. L.; Clancy, P. Mayer Bond Order as a Metric of Complexation Effectiveness in Lead Halide Perovskite Solutions. *Chem. Mater.* **2017**, *29*, 2435−2444.

(10) Nayak, P. K.; Moore, D. T.; Wenger, B.; Nayak, S.; Haghighirad, A. A.; Fineberg, A.; Noel, N. K.; Reid, O. G.; Rumbles, G.; Kukura, P.; Vincent, K. A.; Snaith, H. J. Halide Perovskite Crystals. *Nat. Commun.* **2016**, *7*, 13303.

(11) Noel, N. K.; Habisreutinger, S. N.; Wenger, B.; Klug, M. T.; Hörantner, M. T.; Johnston, M. B.; Nicholas, R. J.; Moore, D. T.; Snaith, H. J. A Low Viscosity, Low Boiling Point, Clean Solvent System for the Rapid Crystallisation of Highly Specular Perovskite Films. *Energy Environ. Sci.* **2017**, *10*, 145−152.

(12) Noel, N. K.; Congiu, M.; Ramadan, A. J.; Fearn, S.; Mcmeekin, D. P.; Patel, J. B.; Johnston, M. B.; Wenger, B.; Snaith, H. J. Joule Unveiling the Underlying Influence of pH on the Crystallization of Hybrid Perovskite Unveiling the Underlying Influence of pH on the Crystallization of Hybrid Perovskite Materials, Delivering Low Voltage Loss Photovoltaics. *Joule* **2017**, *1*, 328−343.

(13) Sun, S.; Yuan, D.; Xu, Y.; Wang, A.; Deng, Z. Ligand-Mediated Synthesis of Shape-Controlled Cesium Lead Halide Perovskite Nanocrystals via Reprecipitation Process at Room Temperature. *ACS Nano* **2016**, *10*, 3648−3657.

(14) Koolyk, M.; Amgar, D.; Aharon, S.; Etgar, L. Kinetics of Cesium Lead Halide Perovskite Nanoparticle Growth; Focusing and de-Focusing of Size Distribution. *Nanoscale* **2016**, *8*, 6403−6409.

(15) Bekenstein, Y.; Koscher, B. A.; Eaton, S. W.; Yang, P.; Alivisatos, A. P. Highly Luminescent Colloidal Nanoplates of Perovskite Cesium Lead Halide and Their Oriented Assemblies. *J. Am. Chem. Soc.* **2015**, *137*, 16008−16011.

(16) Sichert, J. A.; Tong, Y.; Mutz, N.; Vollmer, M.; Fischer, S.; Milowska, K. Z.; García Cortadella, R.; Nickel, B.; Cardenas-Daw, C.; Stolarczyk, J. K.; Urban, A. S.; Feldmann, J. Quantum Size Effect in Organometal Halide Perovskite Nanoplatelets. *Nano Lett.* **2015**, *15*, 6521−6527.

(17) Akkerman, Q. A.; Motti, S. G.; Srimath Kandada, A. R.; Mosconi, E.; D'Innocenzo, V.; Bertoni, G.; Marras, S.; Kamino, B. A.; Miranda, L.; De Angelis, F.; Petrozza, A.; Prato, M.; Manna, L. Solution Synthesis Approach to Colloidal Cesium Lead Halide Perovskite Nanoplatelets with Monolayer-Level Thickness Control. *J. Am. Chem. Soc.* **2016**, *138*, 1010−1016.

(18) Brennan, M. C.; Zinna, J.; Kuno, M. Existence of a Size-Dependent Stokes Shift in CsPbBr$_3$ Perovskite Nanocrystals. *ACS Energy Lett.* **2017**, *2*, 1487−1488.

(19) Shamsi, J.; Dang, Z.; Bianchini, P.; Canale, C.; Di Stasio, F.; Brescia, R.; Prato, M.; Manna, L. Colloidal Synthesis of Quantum Confined Single Crystal CsPbBr$_3$ Nanosheets with Lateral Size Control up to the Micrometer Range. *J. Am. Chem. Soc.* **2016**, *138*, 7240.

(20) Dohner, E. R.; Hoke, E. T.; Karunadasa, H. I. Self-Assembly of Broadband White-Light Emitters. *J. Am. Chem. Soc.* **2014**, *136*, 1718−1721.

(21) Smith, M. D.; Jaffe, A.; Dohner, E. R.; Lindenberg, A. M.; Karunadasa, H. I. Structural Origins of Broadband Emission from Layered Pb-Br Hybrid Perovskites. *Chem. Sci.* **2017**, *8*, 4497−4504.

(22) Bohun, A.; Dolejší, J.; Barta, Č. The Absorption and Luminescence of $(PbCl_6)^{4-}$ and $(PbBr_6)^{4-}$ Complexes. *Czech. J. Phys.* **1970**, *20*, 803−807.

(23) Akkerman, Q. A.; Park, S.; Radicchi, E.; Nunzi, F.; Mosconi, E.; De Angelis, F.; Brescia, R.; Rastogi, P.; Prato, M.; Manna, L. Nearly Monodisperse Insulator Cs_4PbX_6 (X= Cl, Br, I) Nanocrystals, their Mixed Halide Compositions, and their Transformation into $CsPbX_3$ Nanocrystals. *Nano Lett.* **2017**, *17*, 1924−1930.

(24) Liu, Z.; Bekenstein, Y.; Ye, X.; Nguyen, S. C.; Swabeck, J.; Zhang, D.; Lee, S. T.; Yang, P.; Ma, W.; Alivisatos, A. P. Ligand Mediated Transformation of Cesium Lead Bromide Perovskite Nanocrystals to Lead Depleted Cs_4PbBr_6 Nanocrystals. *J. Am. Chem. Soc.* **2017**, *139*, 5309−5312.

(25) Palazon, F.; Almeida, G.; Akkerman, Q. A.; De Trizio, L.; Dang, Z.; Prato, M.; Manna, L. Changing the Dimensionality of Cesium Lead Bromide Nanocrystals by Reversible Postsynthesis Transformations with Amines. *Chem. Mater.* **2017**, *29*, 4167−4171.

(26) Davis, M. M. *Acid−Base Behavior in Aprotic Organic Solvents*; U.S. Department of Commerce, National Bureau of Standards, 1968.

(27) Ravi, V. K.; Santra, P. K.; Joshi, N.; Chugh, J.; Singh, S. K.; Rensmo, H.; Ghosh, P.; Nag, A. Origin of Substitution Mechanism for the Binding of Organic Ligands on the Surface of $CsPbBr_3$ Perovskite Nanocubes. *J. Phys. Chem. Lett.* **2017**, *8*, 4988−4994.

(28) Weidman, M. C.; Goodman, A. J.; Tisdale, W. A. Colloidal Halide Perovskite Nanoplatelets: An Exciting New Class of Semi-conductor Nanomaterials. *Chem. Mater.* **2017**, *29*, 5019−5030.

(29) Maryott, A. A. Conductimetric Titrations of Acids and Bases In Benzene and Dioxane. *J. Res. Natl. Bur. Stand. (1934)* **1947**, *38*, 527−536.

(30) Witschonke, C. R.; Kraus, C. A. Properties of Electrolytic Solutions. XXIX. The Conductance of Some Electrolytes in Nitro-benzene at 25C. *J. Am. Chem. Soc.* **1947**, *69*, 2472−2841.

(31) Coetzee, J. F.; Padmanabhan, G. R. Properties of Bases in Acetonitrile as Solvent. IV. Proton Acceptor Power and Homo-conjugation of Mono- and Diamines. *J. Am. Chem. Soc.* **1965**, *87*, 5005−5010.

(32) Moreels, I.; Fritzinger, B.; Martins, J. C.; Hens, Z. Surface Chemistry of Colloidal PbSe Nanocrystals. *J. Am. Chem. Soc.* **2008**, *130*, 15081−15086.

(33) Moreels, I.; Justo, Y.; De Geyter, B.; Haustraete, K.; Martins, J. C.; Hens, Z. Quantum Dots: A Surface Chemistry Study. *ACS Nano* **2011**, *5*, 2004−2012.

(34) De Roo, J.; Ibáñez, M.; Geiregat, P.; Nedelcu, G.; Walravens, W.; Maes, J.; Martins, J. C.; Van Driessche, I.; Kovalenko, M. V.; Hens, Z. Highly Dynamic Ligand Binding and Light Absorption Coefficient of Cesium Lead Bromide Perovskite Nanocrystals. *ACS Nano* **2016**, *10*, 2071−2081.